Surface & Coatings Technology 432 (2022) 128063

Contents lists available at ScienceDirect

Surface & Coatings Technology

journal homepage: www.elsevier.com/locate/surfcoat

High temperature (900 °C) sliding wear of CrNiAlCY coatings deposited by high velocity oxy fuel thermal spray

K. Derelizade [a], A. Rincon [a], F. Venturi [a], R.G. Wellman [b], A. Kholobystov [c], T. Hussain [a,*]

[a] Faculty of Engineering, University of Nottingham, University Park, Nottingham NG7 2RD, United Kingdom
[b] Surface Engineering, Rolls-Royce plc, Derby DE24 8BJ, United Kingdom
[c] School of Chemistry, University of Nottingham, University Park, Nottingham NG7 2RD, United Kingdom

ARTICLE INFO

Keywords:
HVOF
High temperature
Wear resistance
Nickel alloy

ABSTRACT

Nickel based superalloy are in demand for high temperature applications and their corrosion, erosion and wear resistance have been investigated for a long time. Nickel chromium (NiCr) alloys are widely used for corrosion resistant coatings, while chromium carbide nickel chromium (CrC-NiCr) alloys are preferred for wear resistant coatings at high temperature. In this study CrNiAlCY coatings were deposited via a liquid fuelled high velocity oxy fuel (HVOF) thermal spray using two spray parameters and tested as wear resistant coatings. Effects of processing parameters on microstructure and mechanical properties of the coatings were investigated. Results showed that higher oxygen flow rates are critical for obtaining coatings with lower porosity and higher microhardness. Coating with lower porosity and higher hardness was chosen for both room temperature (~24 °C) and high temperature (900 °C) unlubricated sliding wear tests in a ball on disc setup. The coating was tested against alumina counterbody under 3 different loading conditions (10, 30 and 60 N). The wear rate of the coating was directly proportional to the applied load at room temperature. In the room temperature tests, wear debris was produced, which then oxidised and pushed away to the edges of the wear track. On the other hand, wear debris was smeared on the wear surface at high temperature tests. The surface was oxidised into Cr_2O_3 at high temperatures, which acted as a protective layer. Although thermal softening took place at higher temperatures, wear rates under 10 and 30 N were similar to room temperature values due to the protective oxide layer formed on the top surface; however, the oxide layer under 60 N could not withstand the load, started to crack and lost its protective ability.

1. Introduction

High chromium content nickel-based alloys are widely used in applications as a layer of protective coating, where resistance against high temperature corrosion and wear are required. High chromium content nickel alloys form a continuous Cr_2O_3 layer, which is bonded strongly on the surface at high temperatures to protect the alloy from corrosion and wear. In addition, chromium can also form chromium carbides if carbon is present in the alloy mixture. Chromium carbide has a positive impact on matrix strength and hence improves both corrosion and wear resistance. [1–7]. Aluminium is another common element used in Nickel based super alloys. Ni-Al intermetallics have high melting points and they increase the resistance to oxidation at elevated temperatures. In addition, Ni_3Al intermetallic acts as a strengthening phase in nickel based superalloys [8–10].

Thermal spray is a popular and widely used coating deposition technique in the industry for deposition of wear, erosion and corrosion resistant coatings. It is a cost-effective, fast and reliable way of depositing dense and superior quality coatings with various microstructures at different thickness ranges and from different feedstock materials including nanostructured powders, suspension and solutions [11–14]. In thermal spray, a stream of feedstock powder particles is injected into the flame to gain high velocities and temperatures. Particles are converted into a molten and/or semi-molten state in the flame that are deposited onto a substrate as a result of plastic deformation upon impact at high velocities. There is a wide range of thermal spray techniques available, and they are classified by way of heat source and feedstock types. High velocity oxy fuel (HVOF) thermal spray is a process where oxygen and a fuel are used to create a supersonic combustion jet. In HVOF thermal spray, the fuel can be either a gas (hydrogen, ethylene, propane, etc.) or

* Corresponding author.
E-mail address: Tanvir.Hussain@nottingham.ac.uk (T. Hussain).

https://doi.org/10.1016/j.surfcoat.2021.128063
Received 6 November 2021; Received in revised form 16 December 2021; Accepted 21 December 2021
Available online 4 January 2022

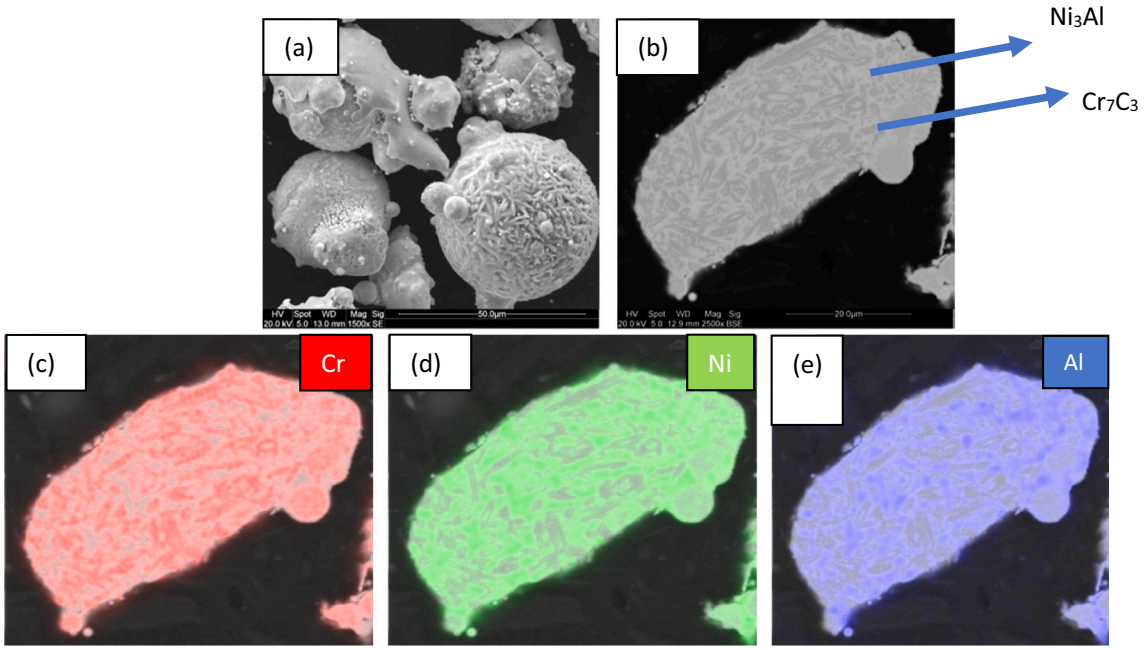

Fig. 1. BSE micrographs showing the CrNiAlCY powder morphology (a) powder cross section (b) and EDX mapping performed on the cross section (c, d and e). Powder has a dendric microstructure confirmed by the EDX. Chromium carbide dendrites, grey phases (c) embedded in a nickel (d) aluminium (e) alloy binder matrix, light grey phases.

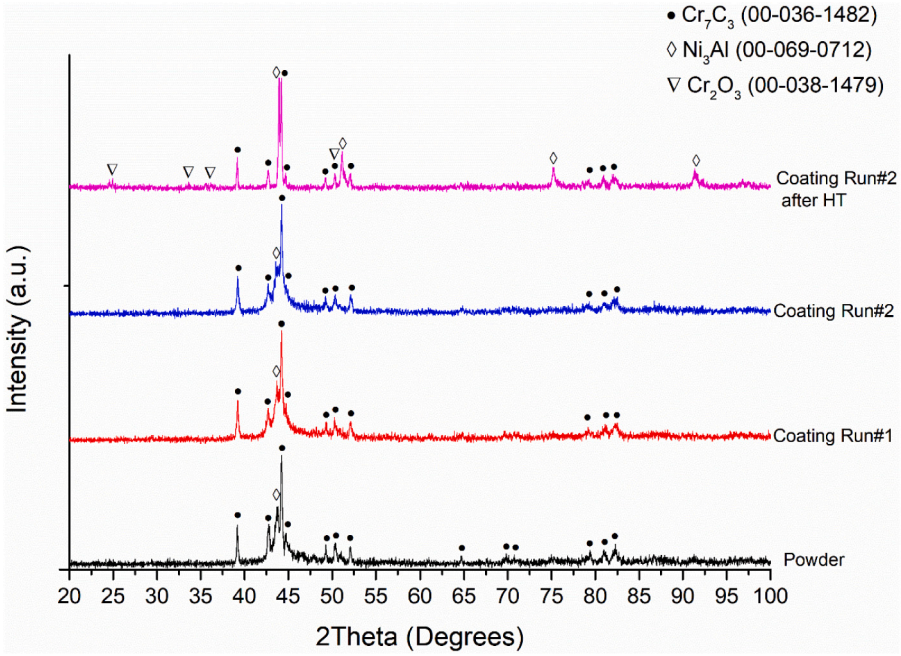

Fig. 2. XRD diffractograms for CrNiAlCY powder, Run#1 coating in as-sprayed condition, Run#2 coating in both as-sprayed and after high temperature exposure conditions.

liquid (kerosene) are injected into a combustion chamber together with oxygen, where an ignition initiates combustion and the exhaust gas travel through a nozzle. Depending on the type of HVOF system, feedstock powders are injected either radially inside the barrel (after the combustion chamber) or axially inside the combustion chamber [15,16]. HVOF thermal spray is the preferred method to deposit dense and well-bonded coatings with a lower degree of decomposition from the metallic feedstocks. Combustion in an HVOF torch generates higher particle velocities with lower temperatures than other thermal spray processes such as plasma spraying [7,15]. This prevents the oxidation, decomposition and decarburisation of the feedstock materials, that can reduce the mechanical properties of the deposited coatings [17–19].

In this study, a recently developed, unique CrNiAlCY powder was characterised and used as a feedstock for the first time in thermal spray process. CrNiAlCY coatings have been produced by changing spray parameters (oxygen flow rate), using a liquid fuelled HVOF thermal spray. This unique alloy was chosen to obtain the combined high matrix strength, corrosion and wear resistance from both chromium carbide and aluminium – nickel intermetallic phases. The microstructure of the deposited coatings was analysed and compared with the initial powder

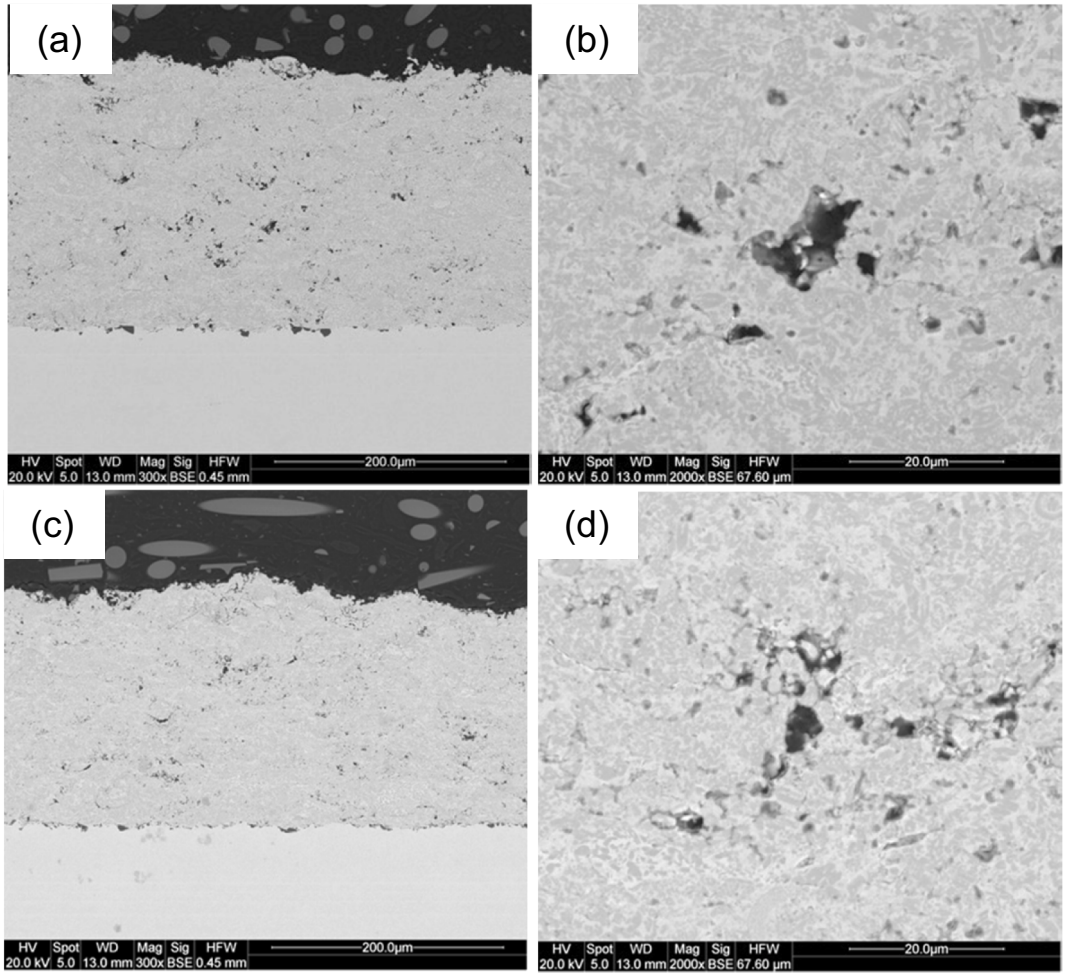

Fig. 3. BSE micrographs of the CrNiAlCY coatings in lower magnification for Run#1 (a) and Run#2 (c) showing uniform thickness and higher magnification for Run#1 (b) and Run#2 (d) showing pores and dendric microstructure of the powder carried on in the coatings as well.

Table 1
Vickers microhardness and porosity values of the coatings deposited from both Run#1, Run#2 and after HT wear test on Run#2. The coating deposited by Run#2 has higher hardness and lower porosity; it was chosen for high temperature wear tests. Oxide phases present in the coating cross sections were also analysed for coatings in as-sprayed and after HT wear conditions.

Sample	Microhardness (HV0.3)	Porosity (%)	Oxide phases (%)
Run#1 As-sprayed	827 ± 15	1.3 ± 0.5	<1.0
Run#2 As-sprayed	974 ± 23	0.4 ± 0.1	<1.0
Run#2 After HT wear	825 ± 24	0.7 ± 0.2	4.0 ± 0.6

to investigate the possibility of this unique powder becoming a metallic feedstock powder candidate for thermal spray applications. Properties of the coatings such as microhardness, porosity and oxide content were investigated and the effect of oxygen flow rate on these properties was studied. Following this analysis, the tribological performance of samples showing the best characteristics was studied at room temperature and at an elevated temperature, using the ball on disc wear test arrangement. The wear performance of the coatings during both room temperature and elevated temperature was investigated and compared to understand their mechanisms. Both properties and wear performance of the best performing coating was investigated for possible usage of this recently developed, unique powder to deposit wear resistant coatings in both room temperature and high temperature applications.

2. Materials & methods

2.1. Powder feedstock & coating deposition

A nickel-chromium-aluminium-based metal powder, CrNiAlCY (Oerlikon Metco, Switzerland) was used in this study. The powder is a recently developed, unique composition and is not yet commercially available. The chemical composition of this metal powder is 45.0–50.0 wt% Chromium (Cr), 39.0–43.0 wt% Nickel (Ni), 6.5–7.2 wt% Aluminium (Al), 4.3–4.7 wt% Carbon (C), 0.14–0.16 wt% Iron (Fe), 0.13–0.15 wt% Yttrium (Y) and 0.01 wt% Silicon (Si). The average particle size (D_{50}) of this metal powder is 31.7 µm. The powder was dried overnight inside a drying cabinet at ~100 °C before the thermal spray to eliminate the moisture and increase the flowability of the powder. Powder flowability was measured according to the ASTM standards B 213–03, which is the time taken to flow a 50 g sample of powder from calibrated orifice funnel (diameter = 2.54 mm).

AISI 304 stainless steel substrates with dimensions of 60 × 25 × 2 mm with nominal composition Fe-19.0Cr-9.3Ni-0.05C (all in wt%) were used as substrates. Substrate surfaces were grit blasted with a blast cleaner from Guyson (Dudley, United Kingdom) at 6 bars with F100 brown aluminium oxide particles (0.125–0.149 mm). Prior to thermal spray, the substrate surfaces were cleaned with industrial methylated spirit (IMS) and compressed air.

Coatings were deposited onto the grit-blasted stainless-steel substrates with a Met-Jet L4 (Metallisation Ltd., England) liquid-fuelled HVOF thermal spray system. Detailed explanation about this thermal

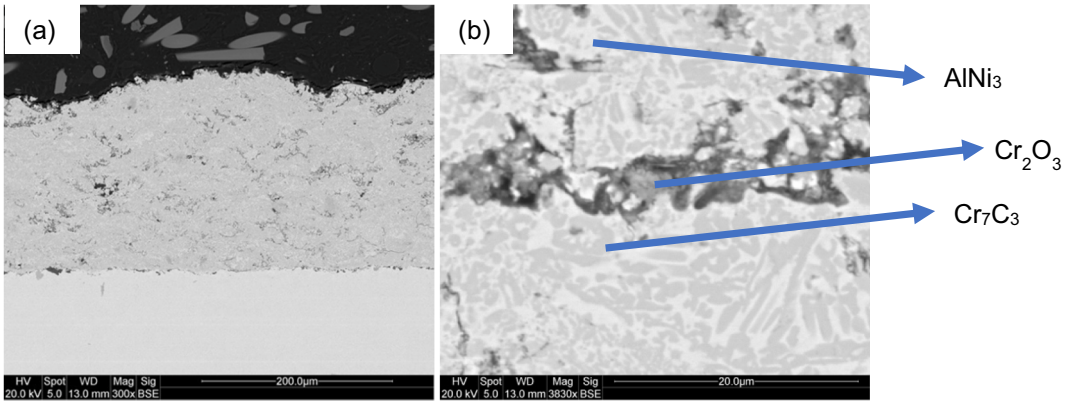

Fig. 4. BSE micrographs of coatings cross section after high temperature exposure in lower (b) and higher (c) magnification. After HT tests, oxide phases were formed in the coating, which can be seen as darker grey phases.

spray setup and schematic can be found in other studies [20,21]. CrNiAlCY powder was injected at a rate of 67.5 g·min^{-1}. Two different spray runs were performed with changing oxygen flow rate from 749 l·min^{-1} (Run#1) to 878 l·min^{-1} (Run#2) while the kerosene flow rate remained constant at 0.445 l·min^{-1}. The higher oxygen flow rate used in Run#2 led to a 100% stoichiometric ratio when combined with 0.445 l·min^{-1} kerosene flow rate. On the other hand, the stoichiometric ratio used in Run#1 was lower than 100% [20]. Stoichiometric ratio is the optimum amount or ratio for a complete combustion reaction, where all the reagents are consumed. Combustion gases and the metal powder were accelerated towards the substrates through a nozzle, which has a length of 100 mm. Substrates were attached to a rotating carousel with a diameter of 260 mm and positioned at a 355 mm stand-off distance. The carousel rotates with a speed of 73 rpm during the spray runs which gives rise to a 1 mm·s^{-1} linear velocity for the attached substrates. Simultaneously, the spray gun moves vertically with a traverse speed of 5 mm·s^{-1}, which leads to a 4 mm overlap between tracks from subsequent passes [22].

2.2. Wear test

Unlubricated rotational sliding wear tests were performed at room temperature (~24 °C) and at an elevated temperature (900 °C). Two different rotary tribometers with a ball on disc arrangement (Ducom Instruments, The Netherlands) were used for these tests. The tribometer used for high temperature was equipped with a built-in furnace. 6 mm alumina (99.9% aluminium oxide) balls (Dejay distributions, United Kingdom) were used as counterbodies, which have a surface finish of 0.038 µm and hardness value of 91 in Rockwell A scale (~2000 HV) as stated by the supplier. Circular wear tracks of 10 mm diameter were created onto the deposited coatings under varying loading conditions (10 N, 30 N and 60 N). As-sprayed samples were used during the wear tests which had a surface roughness (R_a) value of 5.65 ± 0.08 µm. As-sprayed samples were rotated at 100 rpm against the stationary counterbody, giving a linear speed of 52 mm/s. Each test was performed for 2 h and 39 min to reach a total sliding distance of 500 m. Therefore, at elevated temperature wear tests, high temperature exposure of the coatings were 2 h 39 min. Once the tests were completed, coatings were cooled down to room temperature. Two tests were conducted for all conditions.

Volume loss of each wear track was measured at four different points using Talysurf Form 50 contact profilometer (Taylor Hobson, United Kingdom) along with a diamond stylus with a tip radius of 2 µm and lateral resolution of 0.5 µm. Mountains map software (Digital Surf, France) was used to calculate the cross-sectional area of the wear tracks from the line profiles, which were converted into volume loss by multiplying with the circumference of the circular tracks, which is the total length of the wear track [23,24]. In total, eight different points were used to calculate the average and standard error of the mean for each sample. Material volume loss on the counterbody was calculated (from two different measurements – one from each test) by following the assumption of the spherical cap of material removal method reported in the studies [18,25]. The specific wear rate of both the coatings and the counterbodies was calculated from the volume loss, dividing it by applied force and total sliding distance.

2.3. Feedstock, coating and worn surface characterisation

Microstructural characterisation of the powder feedstock, the deposited coatings and the worn surfaces were performed with a Quanta 600 scanning electron microscope, SEM (FEI, The Netherlands) in both SE and BSE modes with 20 kV accelerating voltage using a spot size of 5 and a working distance of 13 mm. EDX software (Bruker, USA) was used for elemental composition analysis. Cross sectional samples of the coatings were prepared by cutting the samples with a diamond cutting disk, followed by sequential silicon carbide (SiC) grinding and diamond polishing with a final grit size of 1 µm. Cross sectional sample for the powder was prepared by hot mounting the powder in the resin and following the same grinding and polishing sequence mentioned above. Both porosity analysis and the oxide content of the coatings were performed on 5 different BSE micrographs for each coating obtained from the SEM at 2000× magnification from the centre of the coatings, which gives rise to an area of 70 µm × 60 µm. Oxides were identified as darker grey phases on the BSE micrographs. Contrast threshold function on ImageJ software [26] was applied to the micrographs according to ASTM E2109 standards to estimate the percentage area fraction in each BSE micrograph. An average value for both porosity and oxide content and the standard mean error were reported in all cases.

X-ray diffraction (XRD) was performed on the CrNiAlCY powder feedstock, deposited coatings and the coating top surface after high temperature wear test to analyse the phase changes. A Bruker D8 Advance diffractometer (Bruker, USA) in θ-2θ Bragg-Brentano geometry was used, the diffractograms were acquired with Cu K_α radiation (1.5406 Å) setting a step size of 0.02° and a time per step of 0.1 s. in the $20° \leq 2\theta \leq 100°$ range.

The coating microhardness was measured via a Vickers microhardness indenter (Buehler, USA) on polished cross sections. 300 gf with a dwell time of 10 s was applied to create 5 indents in the centre of the coatings, parallel to the substrate. The average hardness value with the standard error was reported in all cases.

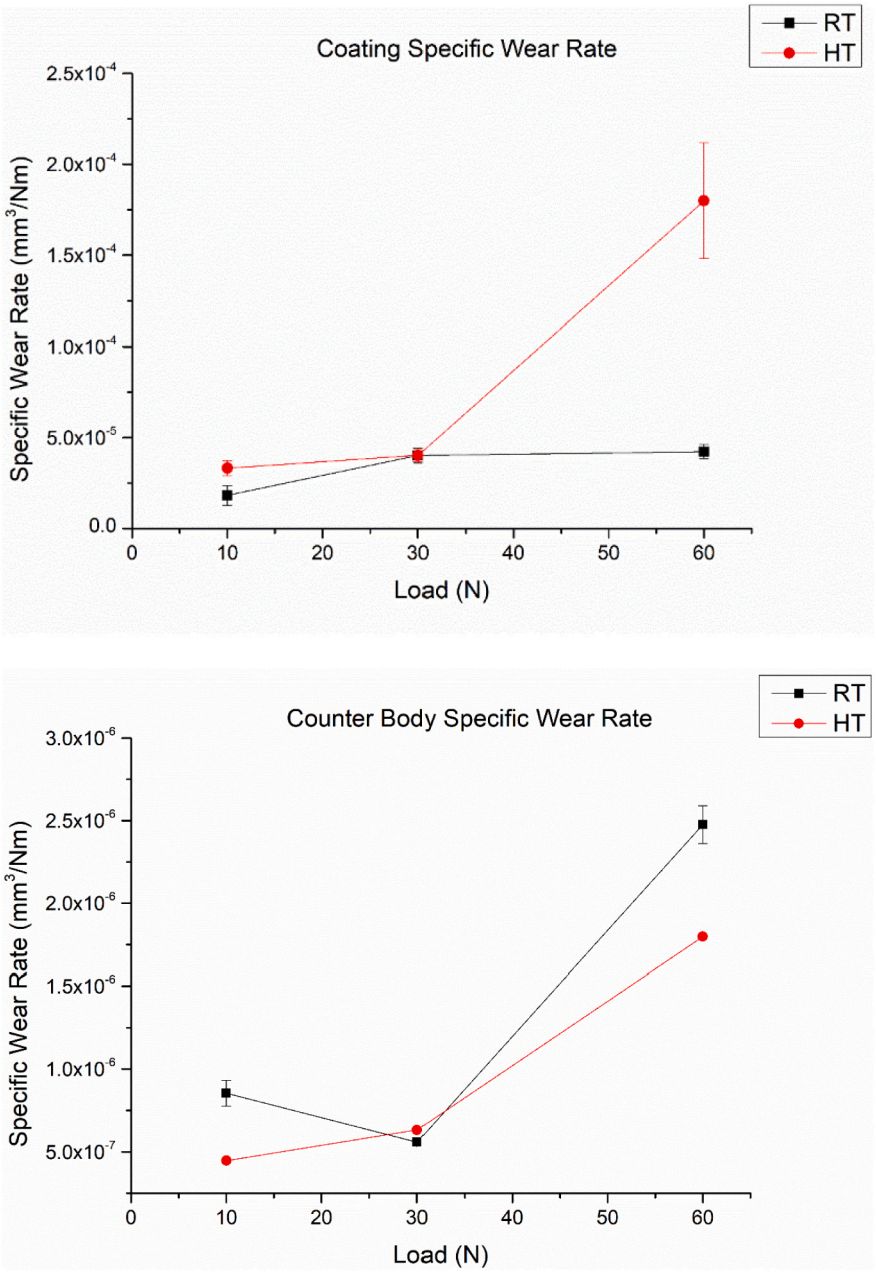

Fig. 5. Specific wear rates of CrNiAlCY coatings at 10, 30 and 60 N in both elevated (900 °C) and room (24 °C) temperatures and corresponding alumina counterbody specific wear rates.

3. Results & discussion

3.1. Feedstock & coating characterisation

Both morphology and cross section of the feedstock metal powder were studied by back scattered electron (BSE) micrographs in conjunction with EDX mapping that are shown in Fig. 1. The feedstock powder has a spheroidal morphology, as can be seen from the Fig. 1a. The powder is free from porosities and it consists of chromium carbide dendrites (grey phases in Fig. 1(b)) embedded in a Nickel and Aluminium alloy (light grey phases in Fig. 1(b)) binder phase. The EDX mapping given in Fig. 1(c, d and e) also confirms the dendric microstructure. XRD diffractogram given in Fig. 2 shows the feedstock powder was composed of mainly Cr_7C_3 and Ni_3Al. The main peak corresponding to Ni_3Al was broad, suggesting that nickel and aluminium alloy binder phase has a lower degree of crystallinity.

BSE micrographs showing cross sections of the coatings produced using different spray parameters (oxygen flow rate 750 l·min^{-1} (Run#1) and 878 l·min^{-1} (Run#2)) are given in Fig. 3. Both coatings had similar thickness values ~220 μm and they showed a good bonding with the substrates. Coating properties, including Vickers microhardness, porosity and oxide content, are given in Table 1. Higher porosity content (dark areas) are detected in Run#1 coating compared to Run#2 coating as can be seen from the lower magnification BSE micrographs, Fig. 3(a, c). Estimated porosity content confirms this, as Run#1 coating had 1.3% ± 0.5 porosity while Run#2 had 0.4% ± 0.1. High magnification BSE micrographs, Fig. 3(b, d), show that both coatings had the same microstructure of the powder feedstock with minimal oxidation. Light grey areas represent aluminium and nickel binder phase, while grey areas represent chromium carbide phases and darker grey areas represents the oxides. Estimated oxide phase content via ImageJ was <1.0%. In this type of HVOF thermal spray system, powder feedstock was

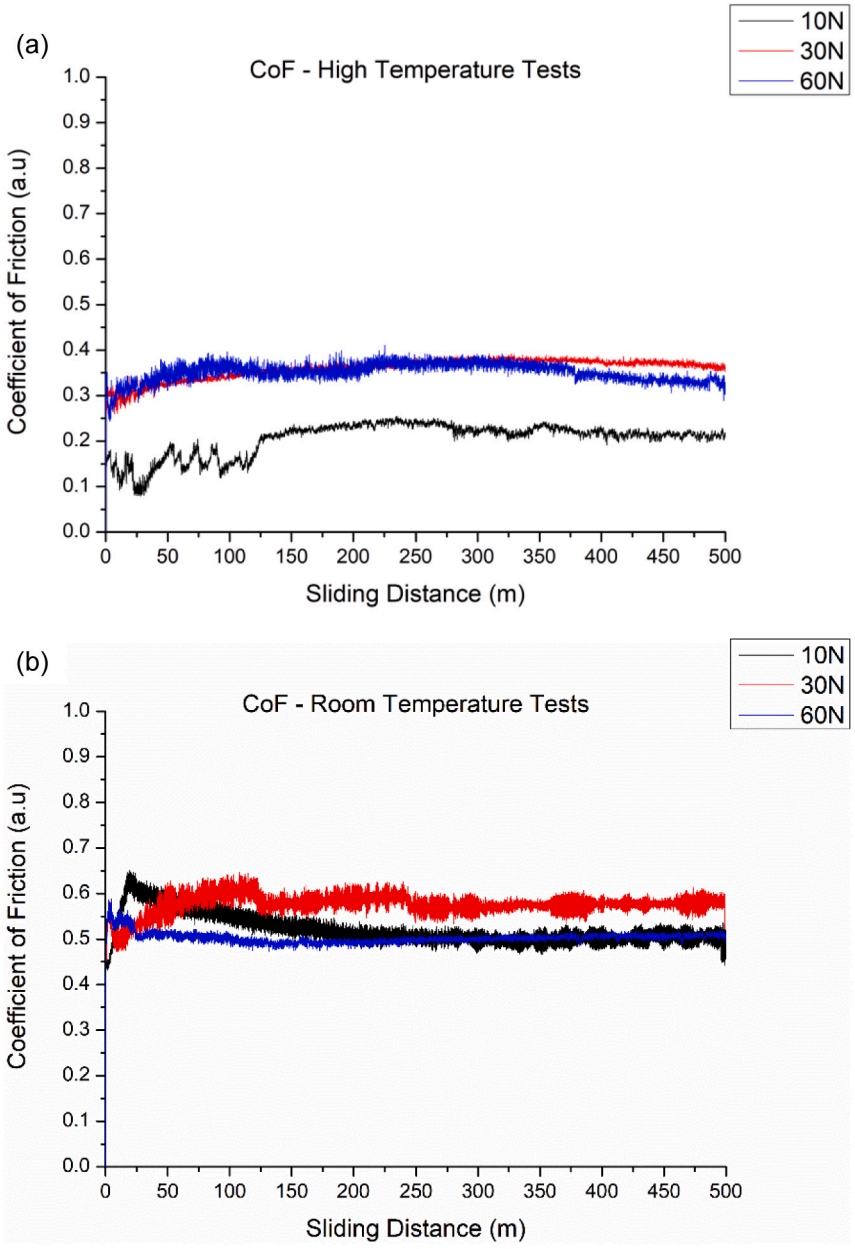

Fig. 6. Coefficient of friction patterns obtained from the wear tests at both high temperature and room temperature wear tests under 10 N, 30 N and 60 N loading conditions.

injected after the combustion chamber. Therefore, the oxidation of the metallic feedstock is prevented, and low oxide content was expected in the final coating. Liquid fueled HVOF thermal spray is the preferred method in the industry to prevent oxidation and decarburisation of the coatings [27].

XRD diffractogram of the as-sprayed coatings shows after thermal spray, chromium carbides remained as Cr_7C_3 together with Ni_3Al and there was no oxide peaks present; however, the peaks are slightly broader compared to the powder feedstock. This was expected as the powder was in a molten phase during thermal spray and fast cooling rates of splats formed on the substrates caused the formation of amorphous and/or nanocrystalline phases. XRD diffractograms together with SEM micrographs confirm that the powder had conserved its microstructure during the thermal spray and there was no significant oxidation of the powder.

Microhardness measurements obtained from both coatings shows that the coatings deposited by Run#2 are harder than that of Run#1. Vickers microhardness for Run#2 coatings was 974 ± 23 HV0.3 while for Run#1 it was only 827 ± 15 HV0.3; however, both coatings presented higher hardness values than nanostructured (727.5 HV0.3) and conventional (456.6 HV0.3) NiCr-Cr_7C_3 coatings deposited by high velocity air fuel (HVAF) technique [4]. Total gas flow was lower during Run#1 as a result of a lower oxygen flow rate. Therefore, velocity and hence the momentum of the particles exiting the nozzle was lower compared to the Run#2. Particles with a lower momentum deform less upon impact with the substrate, which is critical for splat formation and bonding between successive splats [15,16]. As a result, coatings deposited by Run#1 lead to a lower degree of particle deformation, producing weaker intersplat bonds and pores. The difference in oxygen flow rates, explains the reason for increased porosity and reduced hardness for coatings deposited by Run#1. Coatings deposited via Run#2 were chosen for both room temperature and elevated temperature wear tests, as they have improved mechanical properties (higher hardness, lower porosity).

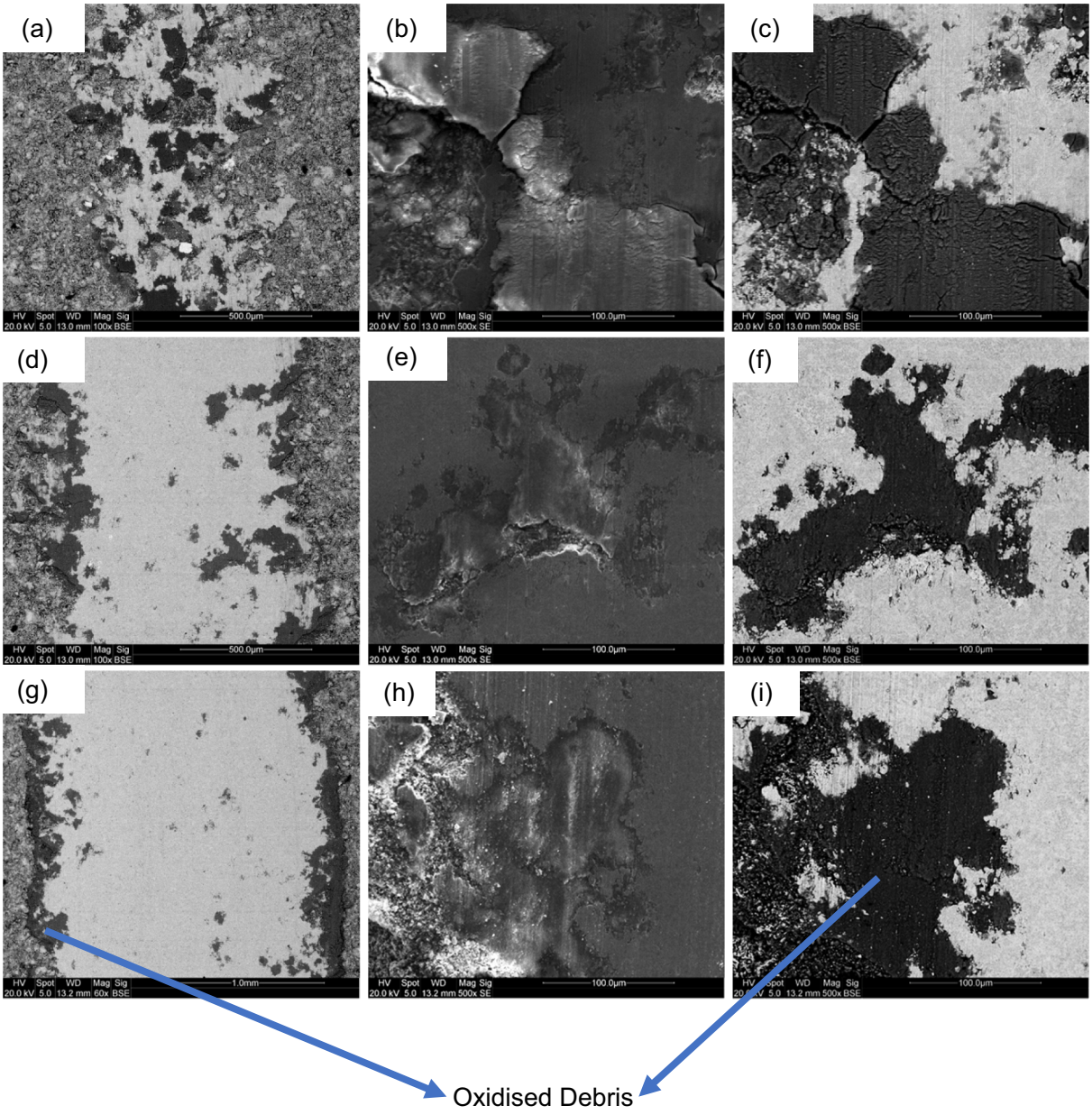

Fig. 7. SEM micrographs of the worn surfaces produced by 10 N (a, b and c), 30 N (d, e and f) and 60 N (g, h and i) at room temperature wear tests. (a, d and g) shows wear tracks width at lower magnifications, while (b, c, e, f, h and i) shows inside the wear track and deformations at higher magnifications in both SE and BSE modes.

To study the effect of temperature on the microstructure without the impact of wear, low and high magnification BSE micrographs of coating Run#2 cross section after high temperature wear test, took far from the wear test zone, are shown in Fig. 4. Coating microstructure looks similar after the high temperature exposure, as the chromium carbides in the aluminium nickel binder phase remained unaltered; however, there is another phase present (darker grey), as can be clearly seen from high magnification BSE micrographs. As a result of high temperature exposure, the coatings oxidised and the oxide phases were randomly disturbed as these darker grey phases can be seen throughout the entire coating cross section. Estimated oxide phase content via ImageJ was increased to 4.0% from <1.0%. XRD diffractogram of the coating after heat treatment also shows the presence of Cr_2O_3, which confirms the oxidation during the high temperature exposure. Cr_7C_3 and Ni_3Al phases are still present. After the heat treatment, the peaks became narrower as a result of the higher degree of crystallisation induced by the temperature. In addition, the intensity of the main Cr_7C_3 peak remained the same (44 2theta), and a carbide phase different than the Cr_7C_3 did not form. Therefore, Cr_7C_3 phase present in the as-sprayed coating did not decarburise after high temperature wear.

After the high temperature exposure, there was a slight increase in porosity content, from 0.4% ± 0.1 to 0.7% ± 0.2. Pores and cracks were present in the coating microstructure around the oxide phases which, could be the reason for a slight increase in porosity. Microhardness of the coating after heat treatment was reduced to 825 ± 24 HV0.3 from 974 ± 23 HV0.3. Nearly 17% reduction in microhardness can be explained as a result of thermal softening, increase in porosity and formation of cracks around the oxides. In addition, some studies reported a reduction in hardness values of the coatings after heat treatment as a result of the reduction in residual stress [28], grain growth and lattice strain relaxation [5].

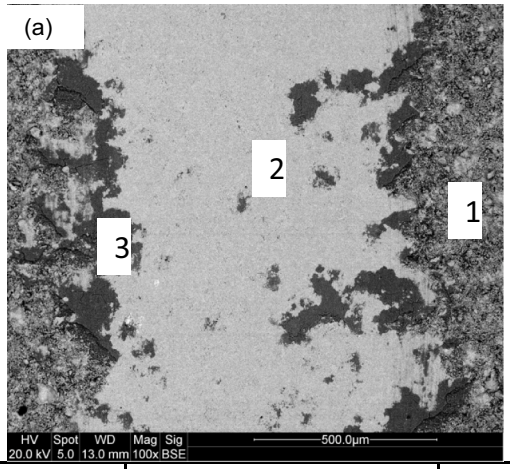

(b)	Point 1- As-sprayed coating surface		Point 2 – Inside the wear track		Point 3- Oxidised wear debris	
Element	wt. %	At.%	wt. %	At.%	wt. %	At.%
Ni	40.4	26.7	41.5	29.3	23.1	9.4
Cr	41.8	31.1	45.6	36.3	23.3	10.5
C	7.8	26.4	7.2	24.9	8.1	15.9
O	2.2	5.3	0.7	1.7	41.3	60.7
Al	7.4	10.7	5.1	7.9	4.0	3.5

Fig. 8. BSE micrograph of the wear track produced by 30 N at RT wear test (a). Smooth and light grey areas are inside the wear track and dark grey areas on the edge of the wear track are the oxidised wear debris. Three points are marked and EDX results from those areas are given (b).

3.2. Wear performance

Wear performance of the coating deposited by Run#2 was investigated under three different loading conditions. Fig. 5 shows the specific wear rates of both coating and alumina counterbody balls against the load for both room temperature (RT) and elevated temperature (HT) tests. The specific wear rate of the coating at room temperature tests was doubled when the loading was increased from 10 N to 30 N. Increase in wear rate was continued for 60 N load as well, but not as much as the jump from 10 N to 30 N. Specific wear rate of the coating is directly proportional to the applied load under room temperature conditions. Under high temperature conditions, the specific wear rate of the coating was similar for both 10 N and 30 N loads. However, the specific wear rate was increased significantly when the loading was increased to 60 N. Overall, the coating achieved lower specific wear rates at room temperature tests compared to elevated temperature ones. Materials are softer at elevated temperatures, and it is easier to deform and create wider and deeper wear tracks. Counterbody specifc wear rates were proportional to the loading. Counterbodies lost more material as the loading increased, 30 N at RT was the only exception. Overall, counterbodies used in RT wear tests lost more material than those used in HT tests. It was expected to obtain less material loss against the coatings at HT as the coatings became softer. Counterbody specifc wear rates were an order of magnitude smaller than the coatings specifc wear rates. Alumina has higher hardness compared to the deposited coatings and its properties are stable at the test conditions used in this study. Therefore, it was expected for alumina counterbodies to be worn less compared to the coatings in both RT and HT wear tests. Fig. 6 shows coefficient of friction graphs averaged over the two repeated tests, obtianed from both high temperature and room temperature wear tests under 10 N, 30 N and 60 N loading conditions. CoF values obtained during the high temperature tests were lower than the corresponding room temperature tests. Resistance to the sliding motion was lower as the materials became softer at higher temperatures. CoF value was stabilised around 0.325–0.350 within the 500 m sliding distance for 30 N and 60 N loads at high temperature tests. However, at 10 N load, CoF value was stable around 0.2 and it fluctuated between 0.1 and 0.2 before reaching a stable state after 100 m sliding distance. The first 100 m was the bedding-in period where the counter body was creating awear track on the top surface of the coating. This period was longer and not uniform as the 10 N load was not high enough to form a uniform wear track as fast as other loading conditions (30 N and 60 N). On the other hand, CoF values at room temperature tests were more consistent for all three loading conditions. CoF values were reached up to 0.6 at some point during the first 100 m for all 3 loading conditions, then stabilised around 0.50–0.55.

SEM micrographs in Fig. 7 shows worn surfaces on the coatings produced at 10 N Fig. 7a, b and c), 30 N (Fig. 7 d, e and f) and 60 N (Fig. 7 g, h and i) at room temperature wear tests. Wear tracks width at lower magnifications can be seen in Fig. 7 (a, d and g) for 10 N, 30 N and 60 N, respectively. Wear track obtained under 10 N loading was not uniform as the loading condition was not high enough to produce a deep wear track. The surface was partially deformed with some unaffected areas. Wear tracks became uniform and wider as the load increased due to the increased applied pressure on the contact point. Worn surfaces at higher magnifications in both SE and BSE modes are shown in Fig. 7 (b and c) for 10 N (e and f) for 30 N and (h and i) for 60 N. Under all loading conditions, deformed surfaces were smooth and polished. There was not any crack, or pull-outs observed. Furthermore, wear debris produced during the tests were oxides due to friction and heat generation between the coating and the counterbody [29]. These can be seen as dark phases on the BSE micrographs. In addition, the amount of oxide debris presents

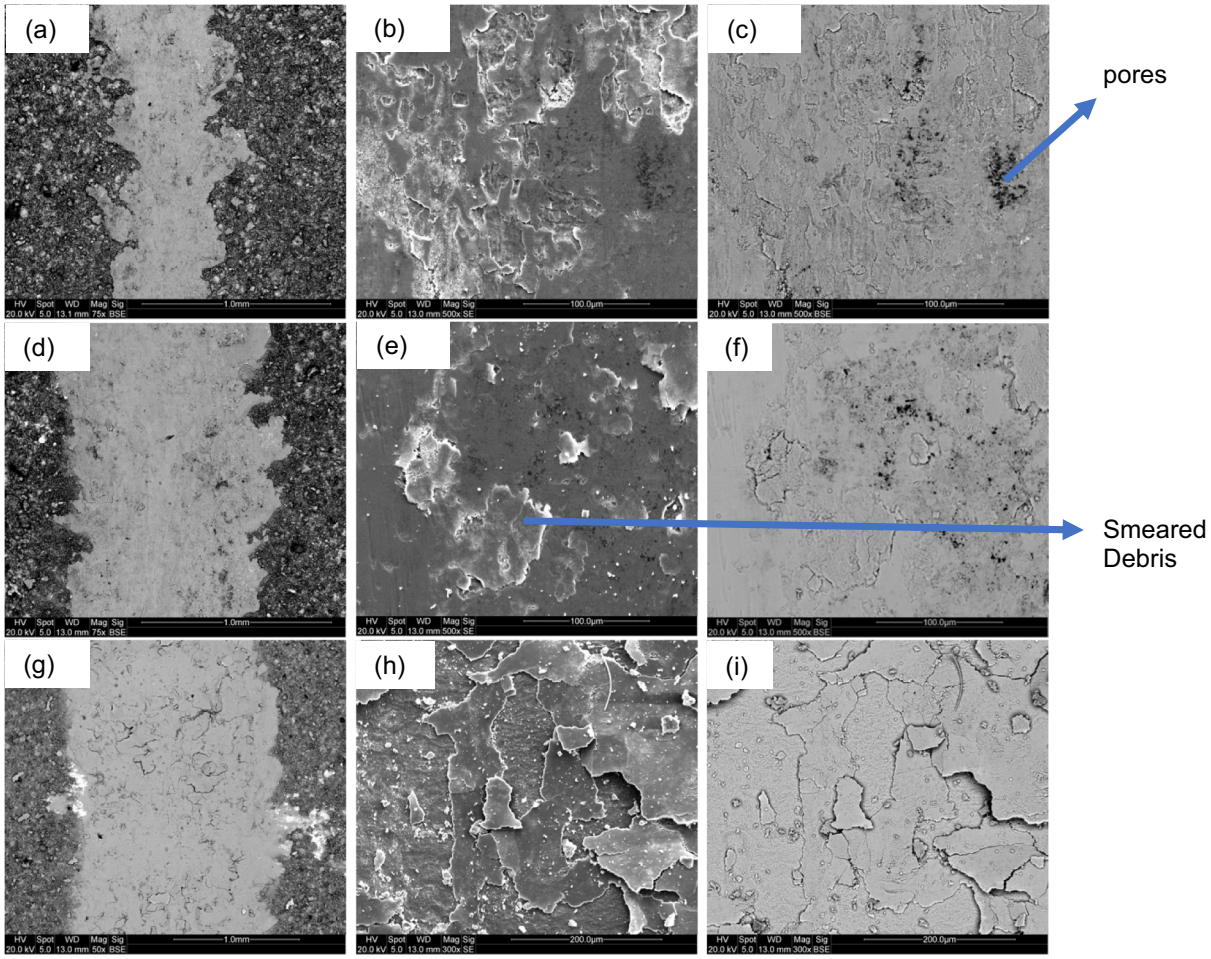

Fig. 9. SEM micrographs of the worn surfaces produced by 10 N (a, b and c), 30 N (d,e and f) and 60 N (g, h and i) at high temperature wear tests. (a, d and g) shows wear tracks width at lower magnifications, while (b, c, e, f, h and i) shows inside the wear track and deformations at higher magnifications in both SE and BSE modes.

inside the wear tracks increased as the loading increased. Oxides were pushed towards the edges of the wear track as they were not strongly bonded to the surface, or there were no pores on the surface to fill with these oxidised debris. 30 N wear track was investigated by EDX and Fig. 8 shows the areas where EDX was performed on the BSE micrographs together with both atomic and weight percentages of elements present. Both wear track surfaces and as-sprayed coating has similar elemental composition suggesting that there was no oxidation on the top surface; however, produced wear debris was oxidised as explained above. There was no oxide present inside the wear track surface labelled as point 2 (light grey phases); however, dark grey phases which were labelled as point 3 were rich in oxides.

SEM micrographs in Fig. 9 shows worn surfaces on the coatings tested at 10 N (Fig. 9a, b and c), 30 N (Fig. 9d, e and f) and 60 N (Fig. 9g, h and i) at high temperature wear tests. Wear tracks width at lower magnifications can be seen in Fig. 9(a, d and g) for 10 N, 30 N and 60 N, respectively. Wear tracks became wider as the load increased due to the increased applied pressure on the contact point. Furthermore, worn surfaces had a smoother finish as the load applied increased. Worn surfaces at higher magnifications in both SE and BSE modes are shown in Fig. 9(b and c) for 10 N (e and f) for 30 N and (h and i) for 60 N. Under 10 N and 30 N loading conditions, surface damage looks similar. Worn surfaces were smoother and peeled off coatings smeared on the surface. Dark phases present on the BSE micrographs represent smaller pores. The coating had similar wear rates at both 10 N and 30 N; therefore, it was expected to have similar deformation on the surfaces. An increase in specific wear rate at 60 N can also be seen from micrographs as the surface deformed significantly more compared to the other loading conditions. The surface was dominantly covered with cracks and delamination of the whole coating top surface took place. The wear track tested at 30 N was investigated by EDX and Fig. 10 shows the areas where EDX was performed on the BSE micrographs together with both atomic and weight percentages of elements present. Both wear track surfaces and as-sprayed coating surfaces had a higher content of oxides compared to room temperature tests. Oxides on top of as-sprayed coating surface were a result of the exposition to elevated temperatures. The ratio between the atomic percentages of chromium and oxygen suggests the formation of Cr_2O_3. This oxide phase was also confirm in XRD diffractogram and reported as the main oxide formed due to high temperature exposure of high chromium content nickel based super alloys in the literature [5,6]. Oxide content inside the wear track surface was slightly higher than the as-sprayed coating surface. Oxidation of the wear track surface resulted from exposure to high temperatures and friction during the wear test. Compared to the room temperature tests, there was not oxidised debris present inside wear tracks. The whole wear track was oxidised during high temperature wear tests and the wear debris produced was smeared onto the surface instead of being pushed towards the edges of the wear track. Elevated temperatures and thermal softening make it easier for the wear debris to bond stronger to the wear track surface. The Cr_2O_3 formed at high temperature acts as a protective layer that prevents the deformation on the top surface; that is why the wear rates at both 10 N and 30 N are similar to the room temperature wear tests. However, at 60 N, the applied load was high enough to damage the protective oxide layer, which can also be seen from SEM

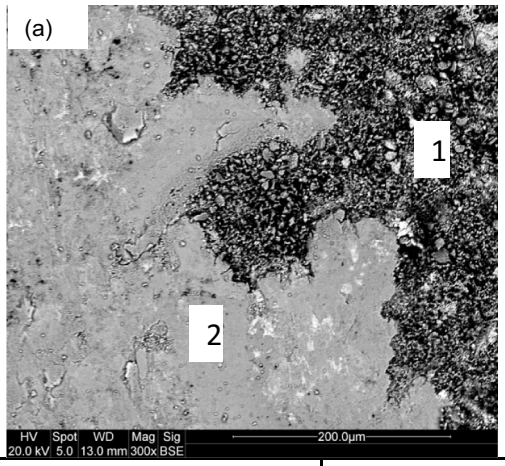

(b)	Point 1- As-sprayed coating surface		Point 2 – Inside the wear track	
Element	wt. %	At.%	wt. %	At.%
Ni	30.7	17.8	32.4	16.3
Cr	43.2	28.2	32.1	18.2
C	3.5	9.8	5.2	12.8
O	18.3	38.8	26.3	48.4
Al	4.1	5.4	4.0	4.4

Fig. 10. BSE micrograph of the wear track produced by 30 N at HT wear test (a). Smooth and light grey areas are inside the wear track and darker grey areas on the edge of wear track are as sprayed coating top surface. Two points were marked and EDX results from those areas are given (b).

micrographs as the top layer of the wear track was full of cracks and flakes. Therefore, the oxide layer was no longer acting as a protective layer and the wear rate at 60 N increased nearly 3 times compared to the room temperature test.

4. Conclusion

In this study, a recently developed unique CrNiAlCY metal powder was characterised and tested as a possible feedstock material for coating deposition by HVOF thermal spray. CrNiAlCY coatings were successfully deposited by HVOF thermal spray using two different oxygen flow rates. Similar coating thicknesses was achieved in both cases and the microstructure of the powder, dendritic chromium carbide grains embedded in an intermetallic aluminium nitride binder matrix was conserved in the coatings. CrNiAlCY coatings deposited using a higher oxygen flow rate (Run#2) achieved increased microhardness and reduced porosity content due to improved mechanical bonding between successive splats. Higher oxygen flow rates are important to achieve higher momentum of particles directed towards the substrate and a higher degree of deformation of splats. Therefore, better mechanical bonding achieved, which leads to denser and harder coatings. However, there was no phase segregation, oxidation or decarburisation in both coating microstructures upon thermal spraying. In addition, coating conserved its microstructure and carbides did not change their forms and decarburise due to high temperature exposure during the high temperature wear tests. These suggest this newly developed unique powder is a good feedstock option for deposition of coatings by HVOF thermal spray for high temperature applications. Wear tests at room temperature showed wear rate increases with the applied loading; however, wear rates at high temperature tests remained similar under 10 N and 30 N loading conditions. The wear rate increased at 60 N only. At room temperature, only wear debris was oxidised and it was pushed away to the edges of the wear track. At higher temperatures, the whole wear surface was oxidised and the wear debris smeared onto the surface instead. Cr_2O_3 oxide was formed at high temperatures, which acted as a protective layer and prevented the deterioration of the surface under both 10 N and 30 N load; however, Cr_2O_3 could not withstand the 60 N load and started to crack and flaked off.

CRediT authorship contribution statement

K. Derelizade: Conceptualization, Methodology, Investigation, Formal analysis, Writing – original draft. **A. Rincon:** Writing – review & editing, Supervision, Formal analysis. **F. Venturi:** Writing – review & editing, Supervision. **R.G. Wellman:** Supervision, Funding acquisition. **A. Kholobysov:** Supervision, Conceptualization, Methodology. **T. Hussain:** Writing – review & editing, Supervision, Conceptualization, Methodology, Project administration.

Declaration of competing interest

The authors declare that they have no known competing financial interests or personal relationships that could have appeared to influence the work reported in this paper.

Acknowledgements

This work was supported by the Engineering and Physical Sciences Research Council [Grant Number EP/M50810X/1]. This work was supported by Rolls-Royce; in the form of a CASE Ph.D. studentship. The authors thank the Nanoscale and Microscale Research Centre (nmRC) for providing access to instrumentations. The authors acknowledge

Heidi Lovelock, Justin Cheney and Jonathon Bracci for supplying the powder. The authors also acknowledge John Kirk at the University of Nottingham for conducting the HVOF thermal spray.

References

[1] D.J. Branagan, M. Breitsameter, B.E. Meacham, V. Belashchenko, High-Performance Nanoscale Composite Coatings for Boiler Applications, (n.d.). doi: 10.1361/10599630523755.
[2] T.S. Sidhu, S. Prakash, R.D. Agrawal, in: Hot corrosion and performance of nickel-based coatings 90, 2006, pp. 41–47 (accessed October 7, 2021), https://about.jstor.org/terms.
[3] J. Singh, H. Vasudev, S. Singh, Performance of different coating materials against high temperature oxidation in boiler tubes - a review, Mater. Today Proc. 26 (2019) 972–978, https://doi.org/10.1016/J.MATPR.2020.01.156.
[4] K. Tao, J. Zhang, H. Cui, X. Lin Zhou, J. Shan Zhang, Fabrication of conventional and nanostructured NiCrC coatings via HVAF technique, Trans. Nonferrous Met. Soc. China 18 (2008) 262–269, https://doi.org/10.1016/S1003-6326(08)60046-1.
[5] K. Tao, X. Zhou, H. Cui, J. Zhang, Microhardness variation in heat-treated conventional and nanostructured NiCrC coatings prepared by HVAF spraying, Surf. Coat. Technol. 203 (2009) 1406–1414, https://doi.org/10.1016/j.surfcoat.2008.11.020.
[6] K. Tao, X. Zhou, H. Cui, J. Zhang, Preparation and properties of a nanostructured NiCrC alloy coating for boiler tubes protection, Mater. Trans. 49 (2008) 2159–2162, https://doi.org/10.2320/matertrans.MRP2008154.
[7] S. Wirojanupatump, P.H. Shipway, D.G. McCartney, The influence of HVOF powder feedstock characteristics on the abrasive wear behaviour of CrxCy–NiCr coatings, Wear 249 (2001) 829–837, https://doi.org/10.1016/S0043-1648(01)00821-3.
[8] M. Durand-Charre, J.H. Davidson, The microstructure of superalloys, 2017, https://doi.org/10.1201/9780203736388.
[9] G.A.L. Opez, S. Sommadossi, W. Gust, E.J. Mittemeijer, P. Zieba, Phase characterization of diffusion soldered Ni/Al/Ni interconnections, Interface Sci. 10 (2002) 13–19.
[10] C. Sims, Superalloys II (extrait), in: Hardcover, J. Wiley & Sons, New York, Chichester, 1987 (accessed November 1, 2021), http://books.google.fr/books?id=kqZTAAAAMAAJ.
[11] D. Tejero-Martin, M. Rezvani Rad, A. McDonald, T. Hussain, Beyond traditional coatings: a review on thermal-sprayed functional and smart coatings, J. Therm. Spray Technol. 28 (2019) 598–644, https://doi.org/10.1007/s11666-019-00857-1.
[12] K. Derelizade, F. Venturi, R.G. Wellman, A. Khlobystov, T. Hussain, Structural changes of thermal sprayed graphene nano platelets film into amorphous carbon under sliding wear, Appl. Surf. Sci. 528 (2020), https://doi.org/10.1016/j.apsusc.2020.146315.
[13] K. Derelizade, F. Venturi, R.G. Wellman, A. Kholobysov, T. Hussain, Wear performance of graphene nano platelets incorporated WC-Co coatings deposited by hybrid high velocity oxy fuel thermal spray, Wear 482–483 (2021), https://doi.org/10.1016/j.wear.2021.203974.
[14] T.S. Sidhu, R.D. Agrawal, S. Prakash, Hot corrosion of some superalloys and role of high-velocity oxy-fuel spray coatings - a review, Surf. Coat. Technol. 198 (2005) 441–446, https://doi.org/10.1016/J.SURFCOAT.2004.10.056.
[15] J.R. Davis, Handbook of thermal spray technology. A. https://app.knovel.com/web/toc.v/cid:kpHTST0006/viewerType:toc, 2004. (Accessed 31 May 2018).
[16] L. Pawlowski, in: The Science and Engineering of Thermal Spray Coatings, Second edition, Sci. Eng. Therm. Spray Coatings Second Ed, 2008, pp. 1–626, https://doi.org/10.1002/9780470754085.
[17] C.J. Li, W.Y. Li, Effect of sprayed powder particle size on the oxidation behavior of MCrAlY materials during high velocity oxygen-fuel deposition, Surf. Coat. Technol. 162 (2003) 31–41, https://doi.org/10.1016/S0257-8972(02)00573-X.
[18] J. Pulsford, S Kamnis, J Murray, M Bai, T Hussain, Effect of Particle and Carbide Grain Sizes on a HVOAF WC-Co-Cr Coating for the Future Application on Internal Surfaces: Microstructure and Wear, J. Therm. Spray Technol. 27 (n.d.). doi: 10.1007/s11666-017-0669-8.
[19] C.J. Li, G.J. Yang, Relationships between feedstock structure, particle parameter, coating deposition, microstructure and properties for thermally sprayed conventional and nanostructured WC-Co, Int. J. Refract. Met. Hard Mater. 39 (2013) 2–17, https://doi.org/10.1016/j.ijrmhm.2012.03.014.
[20] B. Song, M Bai, K T Voisey, T Hussain, Role of Oxides and Porosity on High-Temperature Oxidation of Liquid-Fueled HVOF Thermal-Sprayed Ni50Cr Coatings, J. Therm. Spray Technol. 26 (n.d.). doi:10.1007/s11666-017-0531-z.
[21] B. Song, Z. Pala, K.T. Voisey, T. Hussain, Gas and liquid-fuelled HVOF spraying of Ni50Cr coating: microstructure and high temperature oxidation, Surf. Coat. Technol. 318 (2017) 224–232, https://doi.org/10.1016/j.surfcoat.2016.07.046.
[22] M. Bai, H. Maher, Z. Pala, T. Hussain, Microstructure and phase stability of suspension high velocity oxy-fuel sprayed yttria stabilised zirconia coatings from aqueous and ethanol based suspensions, J. Eur. Ceram. Soc. 38 (2018) 1878–1887, https://doi.org/10.1016/j.jeurceramsoc.2017.10.026.
[23] T. Sudaprasert, P.H. Shipway, D.G. McCartney, Sliding wear behaviour of HVOF sprayed WC-co coatings deposited with both gas-fuelled and liquid-fuelled systems, Wear 255 (2003) 943–949, https://doi.org/10.1016/S0043-1648(03)00293-X.
[24] P.H. Shipway, D.G. McCartney, T. Sudaprasert, Sliding wear behaviour of conventional and nanostructured HVOF sprayed WC-Co coatings, Wear 259 (2005) 820–827, https://doi.org/10.1016/j.wear.2005.02.059.
[25] P.H. Shipway, The role of test conditions on the microabrasive wear behaviour of soda-lime glass, in: Wear, Elsevier, Sequoia SA, 1999, pp. 191–199, https://doi.org/10.1016/S0043-1648(99)00187-8.
[26] C.A. Schneider, W.S. Rasband, K.W. Eliceiri, NIH image to ImageJ: 25 years of image analysis, Nat. Methods 9 (2012) 671–675, https://doi.org/10.1038/nmeth.2089.
[27] R. Schwetzke, H. Kreye, Microstructure and properties of tungsten carbide coatings sprayed with various high-velocity oxygen fuel spray systems, J. Therm. Spray Technol. 8 (1999) 433–439, https://doi.org/10.1361/105996399770350395.
[28] W. Herr, E. Broszeit, The influence of a heat treatment on the microstructure and mechanical properties of sputtered coatings, Surf. Coat. Technol. 97 (1997) 335–340, https://doi.org/10.1016/S0257-8972(97)00196-5.
[29] G. Straffelini, Wear mechanisms, in: Springer Tracts Mech. Eng, 2015, https://doi.org/10.1007/978-3-319-05894-8_4.